Phasing and climate forcing potential of the Millennium Eruption of Mt. Baekdu

Giyoon Lee[1], Andrea Burke[2], William Hutchison[2], Patrick Sugden[2], Celeste Smith[2], Joseph R. McConnell[3], Michael Sigl[4], Clive Oppenheimer[5,6], Sune Olander Rasmussen[7], Jørgen Peder Steffensen[7], Seung Ryeol Lee[8], Jinho Ahn[1*]

Supplementary Information

Supplementary Note 1. Additional cryptotephra findings

In our study, we focused on tephra populations which we defined as multiple shards in the same sub-sample with a near identical chemistry on all major elements. In addition to the Baekdu shards described in the main text we also identified tephra populations in T3 and T7 (Supplementary Data 1). To identify a potential candidate for these eruptions we first looked at source region, based on large compilations of glass geochemical data from Alaska, Iceland, Japan, and Kamchatka (Supplementary Fig. 11). This shows that Alaska, Iceland, and Kamchatka are all credible source regions.

We next looked at NH eruptions that occurred within the time frame of 945–950 CE (Supplementary Table 3). Through the comparison of chemical composition, the only overlap was with proximal ash deposit of Mt. Rainier[1] (Supplementary Fig. 12). In Supplementary Figure 13, we present the major element chemistry data of an eruption of Mt. Rainer that has been dated to approximately 1,040 ± 410 cal years BP[1] (cal year refers to radiocarbon ages calibrated to calendar year; BP, before the present). This corresponds to the time period of 910 ± 410 CE and overlaps our precise ice core age of 946–947 CE. A good match is seen on most major elements, although there is offset on MgO (Supplementary Fig. 13).

Various types of potential tephra shards were also found in sample T6, T8, T9, and T10, but are unclear whether they are a primary tephra deposit because there are only one or two shards, chemistries were not consistent between shards, and Na was too low for fresh glass. Plunkett et al.[2] suggested that a rhyolite shard discovered together with the ME tephra in the NEEM-2011-S1 ice core by Sun et al.[3] (referred to as QUB-1819c) (Fig. 1), likely originated from volcanoes nearby Japan. A single shard that has similar chemistry with the QUB-1819c was found in T8 (Supplementary Data 1). A rhyolite shard found in sample T10 closely resembled the ME fallout (Supplementary Data 1), which may represent either a primary volcanic ashfall[4] from another rhyolitic volcanic eruption or resuspension of ME fallout.

Table S1. Discrete measurement results of sulfur concentration and isotope data from NGRIP1 ice core samples and estimated volcanic fractions and its sulfur isotopic ratio.

Top Depth (m)	Bottom Depth (m)	S (ppb)	$\delta^{34}S$	$\delta^{34}S$ error (2σ)	$\delta^{33}S$	$\delta^{33}S$ error (2σ)	$\Delta^{33}S$	$\Delta^{33}S$ error (2σ)	f_{volc}	f_{volc} error (2σ)	$\delta^{34}S_{volc}$	$\delta^{34}S_{volc}$ error (2σ)	$\delta^{33}S_{volc}$	$\delta^{33}S_{volc}$ error (2σ)	$\Delta^{33}S_{volc}$	$\Delta^{33}S_{volc}$ error (2σ)	Sample name
217.800	217.950	15.1	6.82	0.11	3.43	0.11	-0.07	0.09									T10
217.950	218.050	15.6	7.87	0.11	4.07	0.11	0.03	0.09									T9
218.050	218.150	14.7	7.72	0.11	4.02	0.11	0.05	0.09									
218.150	218.250	12.7	8.53	0.11	4.43	0.11	0.05	0.09									
218.250	218.350	15.2	7.32	0.11	3.73	0.11	-0.03	0.09									T8
218.350	218.400	24.0	6.91	0.11	3.65	0.11	0.09	0.09	0.60	0.11	4.57	1.20	2.47	0.60	0.12	0.33	
218.400	218.450	20.2	6.92	0.11	3.54	0.11	-0.02	0.09									T7
218.450	218.475	38.3	6.42	0.11	3.30	0.11	0.00	0.09	0.75	0.07	5.12	0.54	2.62	0.28	-0.01	0.17	T6
218.475	218.500	60.8	6.63	0.11	3.45	0.11	0.04	0.09	0.84	0.05	5.95	0.29	3.10	0.16	0.04	0.12	T5
218.500	218.550	24.3	6.92	0.11	3.51	0.11	-0.04	0.09	0.61	0.10	4.64	1.15	2.27	0.62	-0.11	0.32	T4
218.550	218.650	17.1	7.34	0.11	3.82	0.11	0.05	0.09									T3
218.650	218.750	14.3	8.32	0.11	4.25	0.11	-0.03	0.09									T2
218.750	218.900	9.5	10.21	0.11	5.30	0.11	0.06	0.09									T1

Table S2. The monthly net accumulation rate and values used for the annual net accumulation model. Monthly net accumulations were derived based on Shuman et al.[5].

Days after 1 November	Date	Monthly net accumulation (mm)	Uncertainty (1 σ)	Fraction of annual net accumulation	Uncertainty (1 σ)
0	01-Nov.			0.000	0.000
30	01-Dec.	11.23	0.80	0.055	0.012
61	01-Jan.	11.30	1.72	0.115	0.013
92	01-Feb.	11.22	1.08	0.174	0.016
120	01-Mar.	11.72	2.82	0.233	0.018
151	01-Apr.	13.98	0.38	0.294	0.021
182	01-May	15.71	1.21	0.367	0.023
212	01-Jun.	22.79	2.44	0.450	0.026
242	01-Jul.	19.53	1.81	0.571	0.030
274	01-Aug.	18.47	1.35	0.673	0.033
304	01-Sept.	22.93	6.85	0.771	0.037
334	01-Oct.	21.86	5.74	0.887	0.028
365	01-Nov.	10.55	2.19	1.000	0.000

Table S3. Candidate volcanic eruptions in the northern hemisphere representing the tephra shards found in NGRIP1 ice core (based on the Smithsonian Institution Global Volcanism Program).

Volcano name	Country	Eruption year (CE)	Latitude	Longitude	VEI	Reference for chemical composition of proximal fallouts or tephra shards
Edziza	Canada	950 ± 1000	57.72	-130.63	3	(6)
Ljósufjöll	Iceland	960 ± 10	64.90	-22.48	3	(7)
Oddnyjarhnjukur-Langjokull	Iceland	950 ± 50	64.85	-19.70	2	Smithsonian Institution Global Volcanism Program https://volcano.si.edu/
Bárðarbunga (Veiðivötn)	Iceland	940 (?)	64.63	-17.52	-	(8)
Brennisteinsfjöll	Iceland	910 ± 75 950 (?)	63.93	-21.78	2 2	(9)
Katla	Iceland	950 (?)	63.63	19.08	3	(10)
Adatarayama	Japan	950 ± 50	37.65	140.28	-	Japan Meteorological Agency, 2013. https://www.data.jma.go.jp/vois/data/tokyo/STOCK/souran_eng/menu.htm
Kirishimayama	Japan	945	31.93	130.86	2	Japan Meteorological Agency, 2013. https://www.data.jma.go.jp/vois/data/tokyo/STOCK/souran_eng/menu.htm
Kuchinoerabujima	Japan	970 ± 75	30.44	130.22	-	Japan Meteorological Agency, 2013. https://www.data.jma.go.jp/vois/data/tokyo/STOCK/souran_eng/menu.htm
Akan	Japan	950 (?)	43.38	144.01	-	(11)
Tokachidake	Japan	950 ± 50	43.42	142.69	-	(12)
Terceira	Portugal	920 ± 50	38.73	-27.32	-	(13)
Picos Fissural Volcanic System	Portugal	940 ± 100	37.78	-25.67	-	(14)
Sete Cidades	Portugal	950 ± 100	37.87	-25.79	2	(14)
Karymsky	Russia	950 (?)	54.05	159.44	-	(15)
Mutnovsky	Russia	950 (?)	52.45	158.20	2	(16)
Shiveluch	Russia	970 (?) ± 80	56.65	161.36	4	(17)

Tolbachik	Russia	950 (?)	55.83	160.33	4	(18)
Bezymianny	Russia	950 (?)	55.97	160.60	4	(18)
Kikhpinych	Russia	900 ± 50	54.49	160.25	3	(19)
Glacier Peak	US	900 ± 50	48.11	-121.11	3	(20)
Lassen Volcanic Center	US	980 ± 300 880 ± 300 800 ± 300	40.49	-121.51	-	(21)
Shishaldin	US	950 (?)	54.76	-163.97	-	(22)
Augustine	US	930 ± 150	59.36	-153.43	-	(23)
Jefferson	US	950 (?)	44.67	-121.80	-	(24)
Rainier	US	910 ± 410	46.85	-121.76	2	(1)
Adams	US	950 (?)	46.21	-121.49	2	(25)

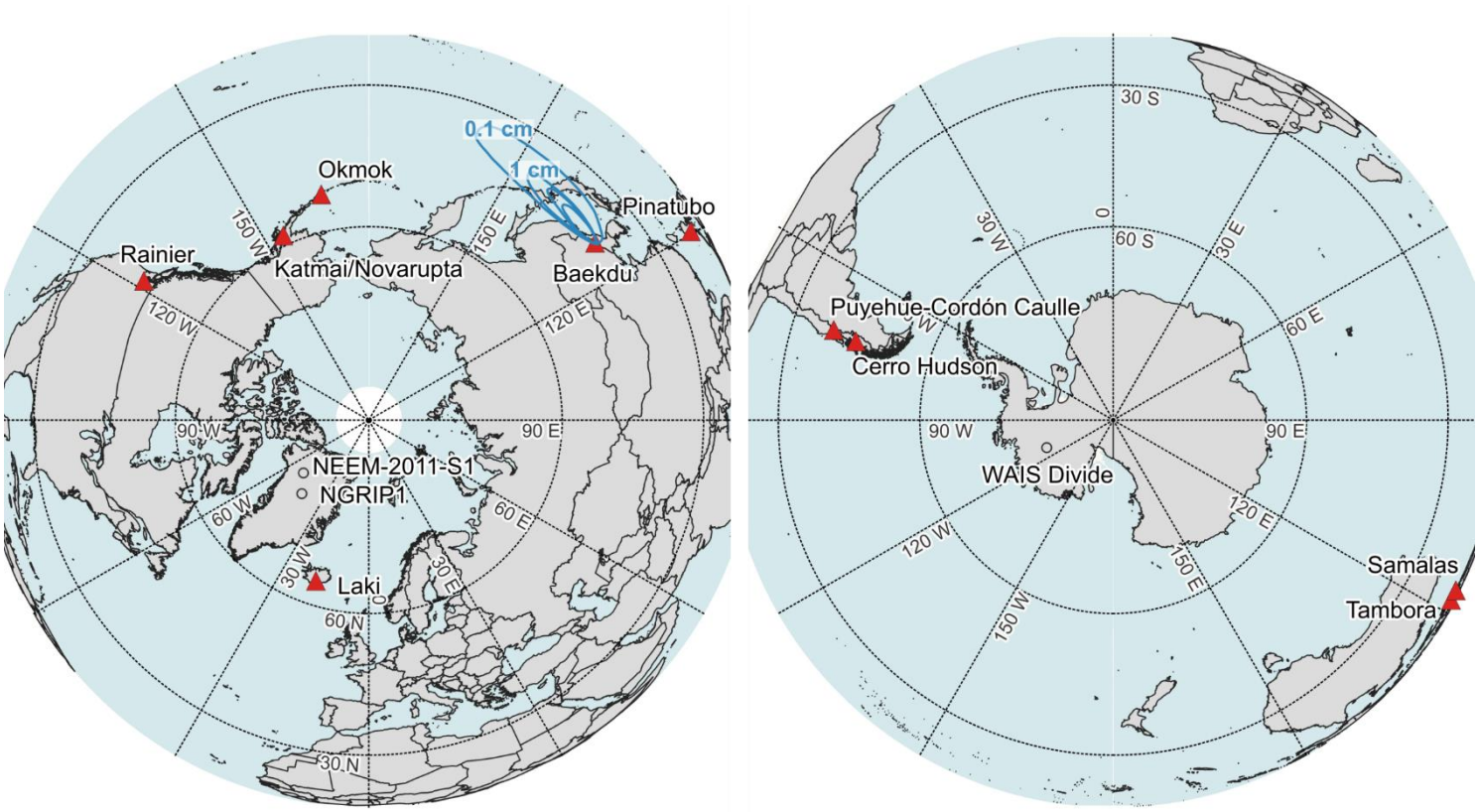

Figure S1. Location of volcanoes and ice-core sites (NEEM-2011-S1, NGRIP1, and WAIS Divide) discussed in the text. Isopachs of ME (blue line) are from Yang et al.[26]. 1 cm and 0.1 cm indicate the thickness of the isopachs.

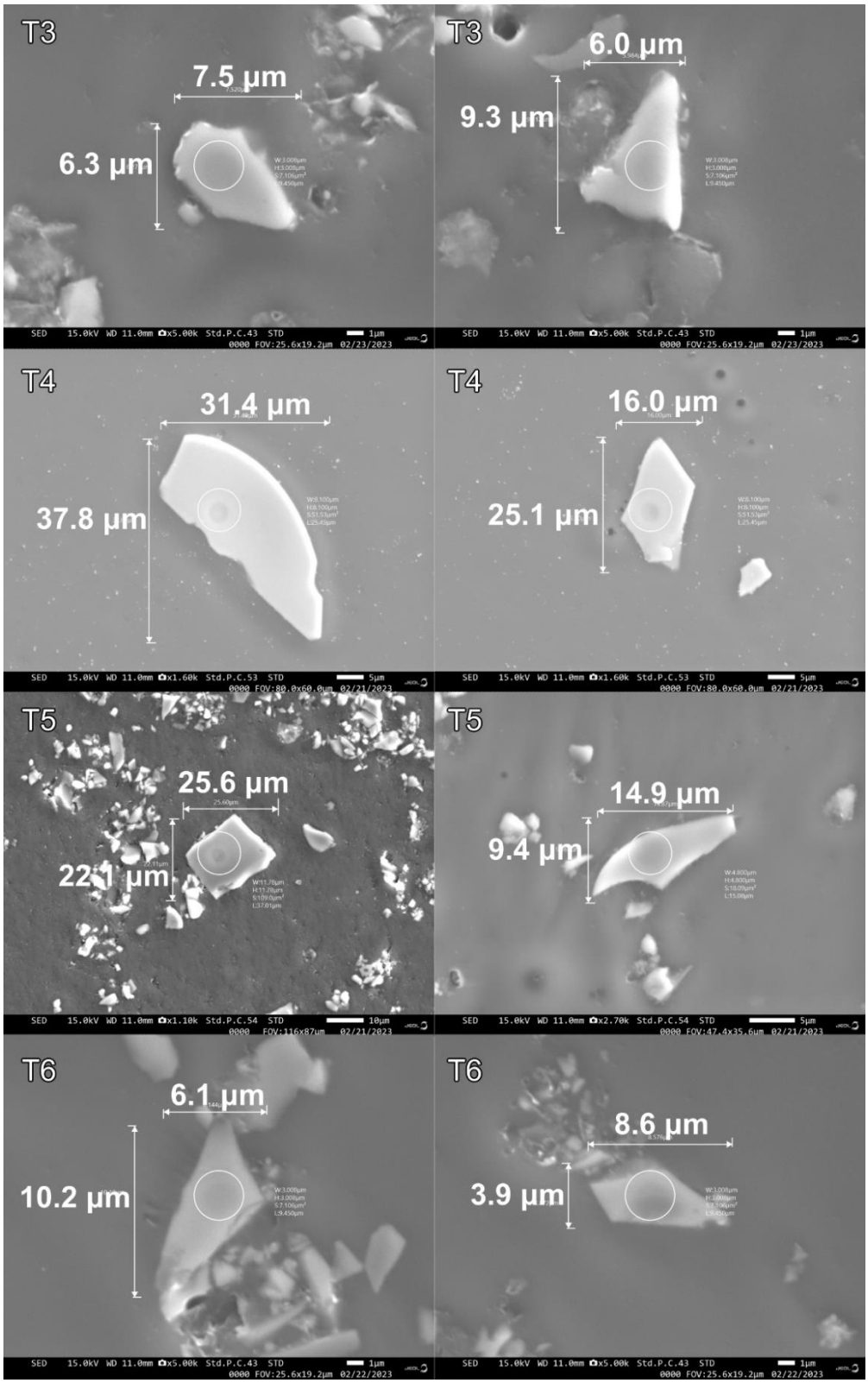

Figure S2. Several tephra shard images found in sample from T3 to T6 from NGRIP1 ice-core. Images were acquired by scanning electron microscopy (SEM) using either the secondary electron detector (SED).

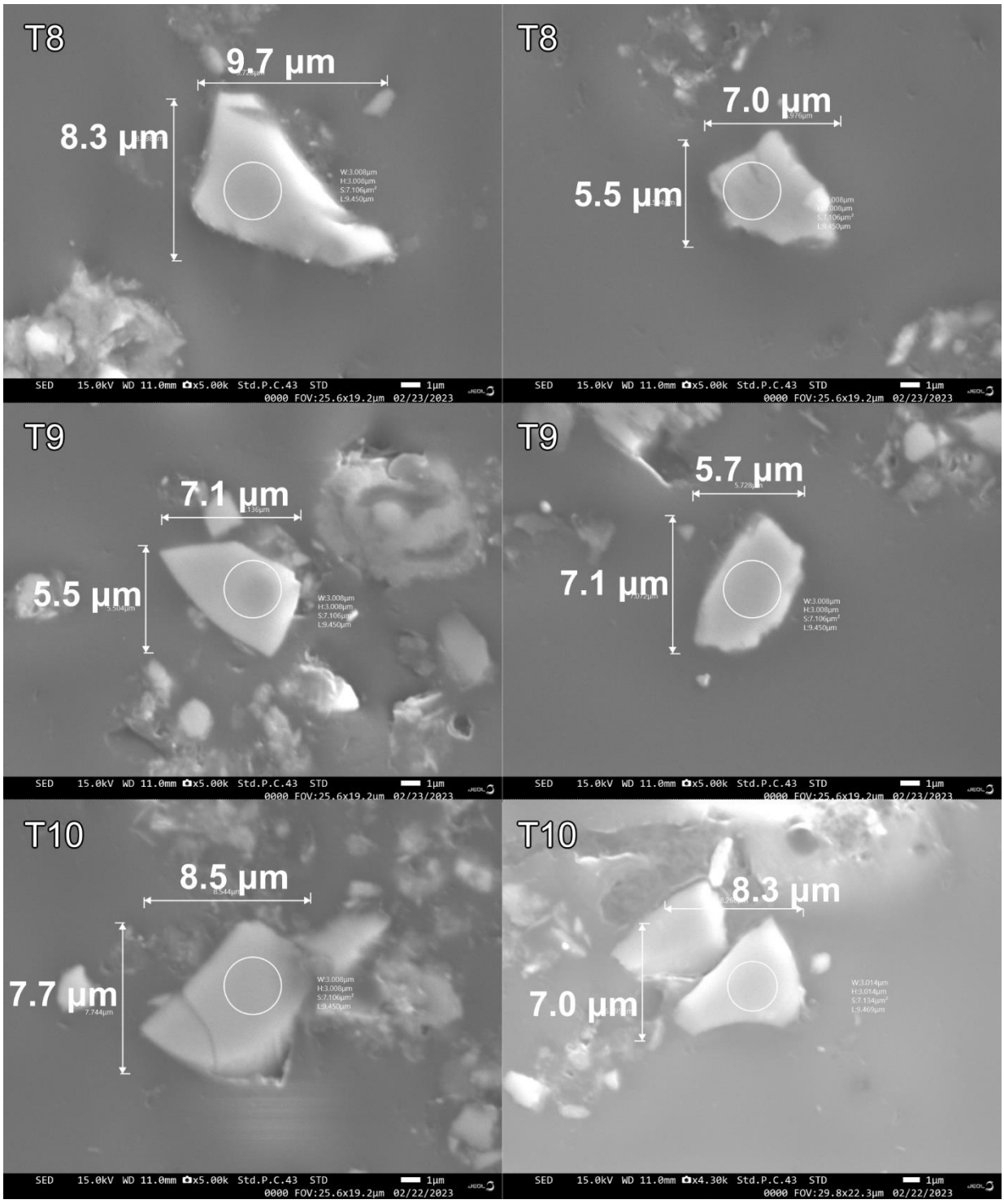

Figure S3. Several tephra shard images found in sample from T8 to T10 from NGRIP1 ice-core. Images were acquired by scanning electron microscopy (SEM) using either the secondary electron detector (SED).

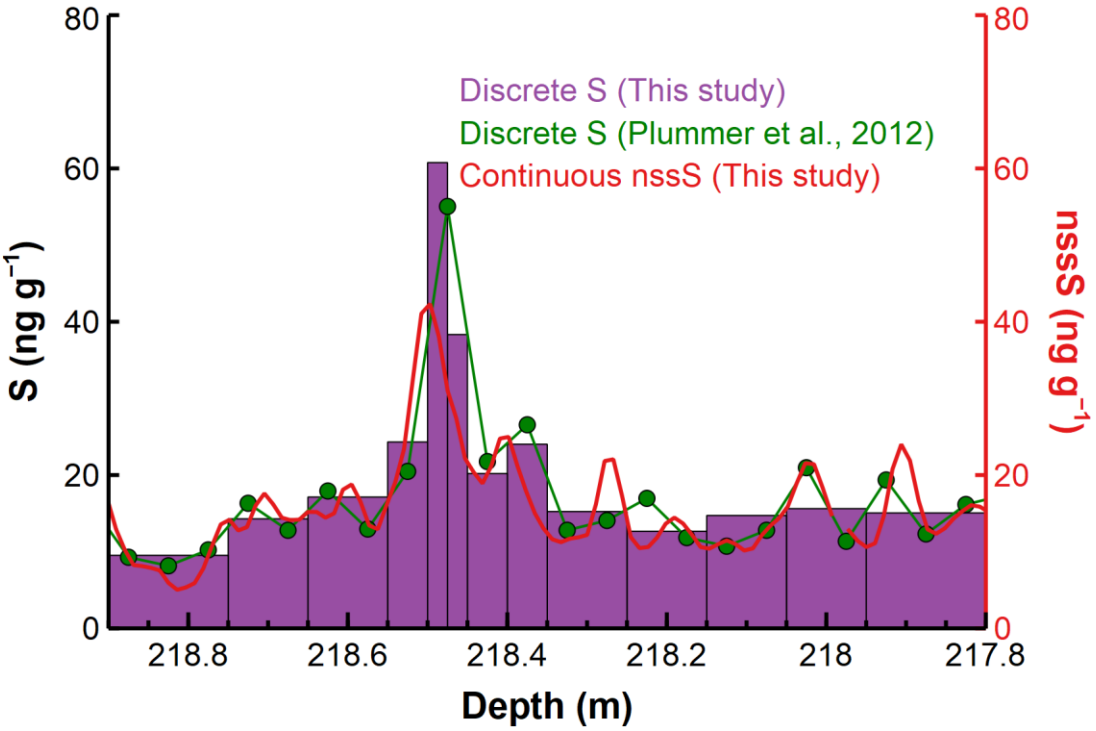

Figure S4. Comparison of sulfur concentrations with previously published ones[27].

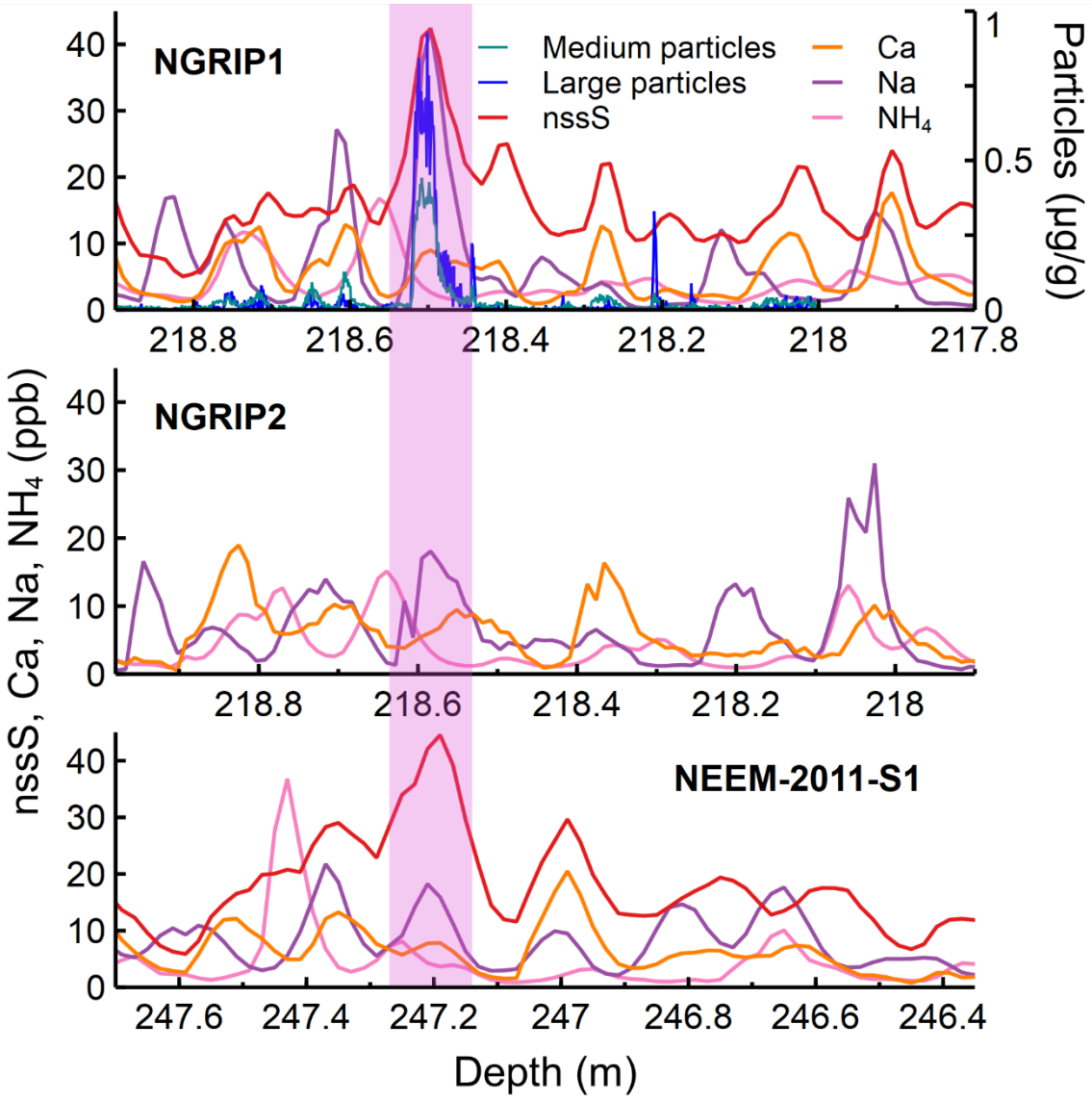

Figure S5. Various ions and insoluble particle concentrations. The pink vertical bar covers the depth range corresponding to the ME. **(a)** Results of NGRIP1 (This study). **(b)** Results of NGRIP2 are from McConnell[28]. **(c)** Results of NEEM-2011-S1 are from Sigl et al.[29].

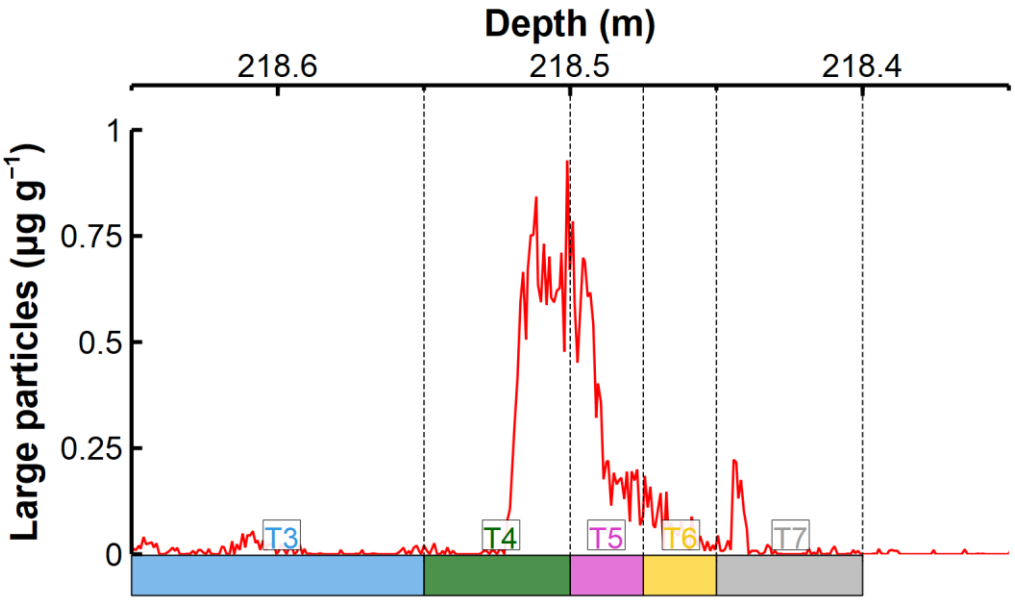

Figure S6. DRI measurements of insoluble particle concentrations of NGRIP1. T3 to T7 represent consecutive ice samples for tephra shard analysis, with corresponding depths shown at the bottom of the panel.

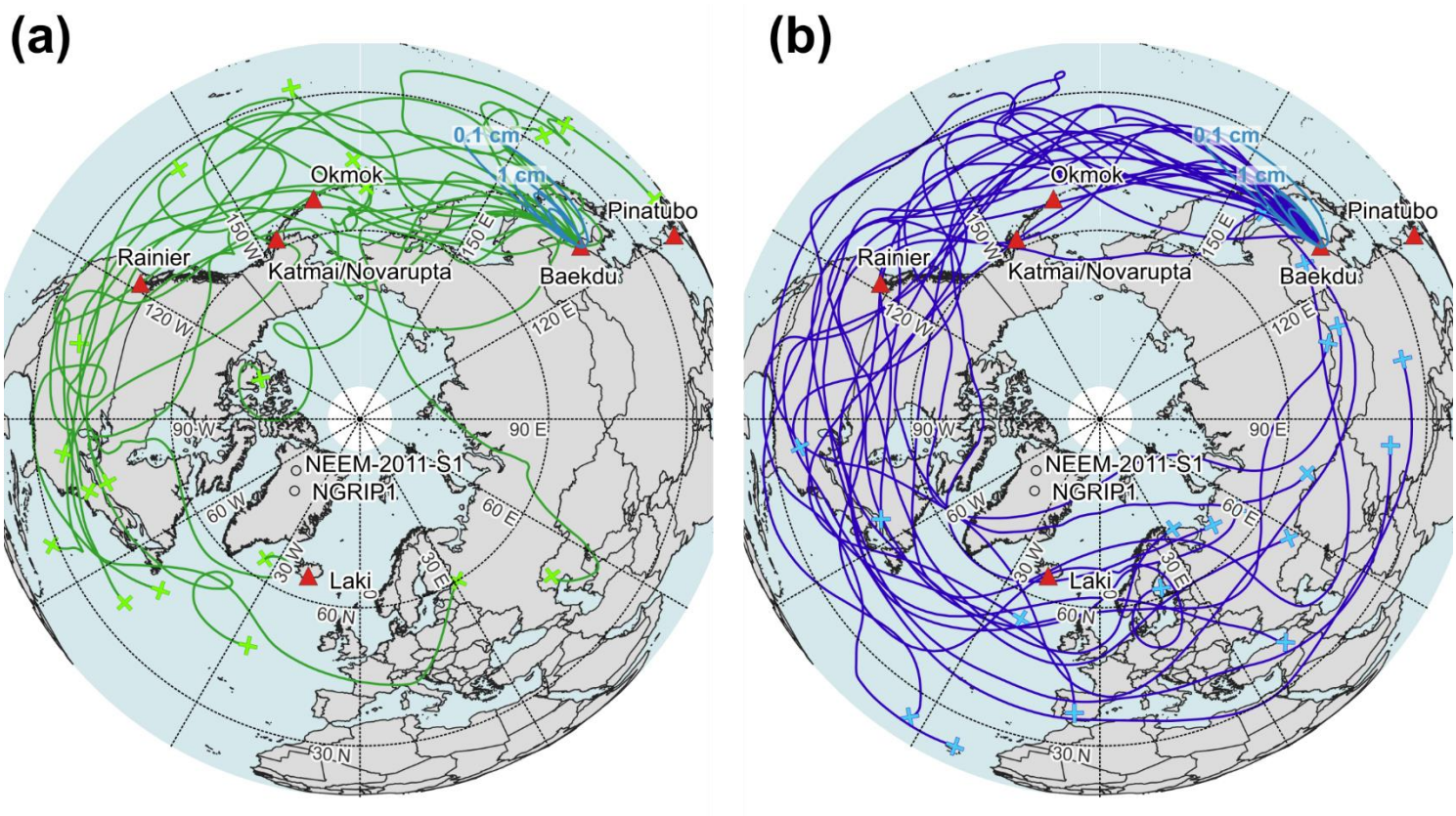

Figure S7. The 240-hour forward air-trajectory of 1 November from 2005 to 2023. **(a)** Starting heights of 8 km above mean sea level (AMSL) and **(b)** 14 km AMSL. The cross symbols represent the endpoint locations.

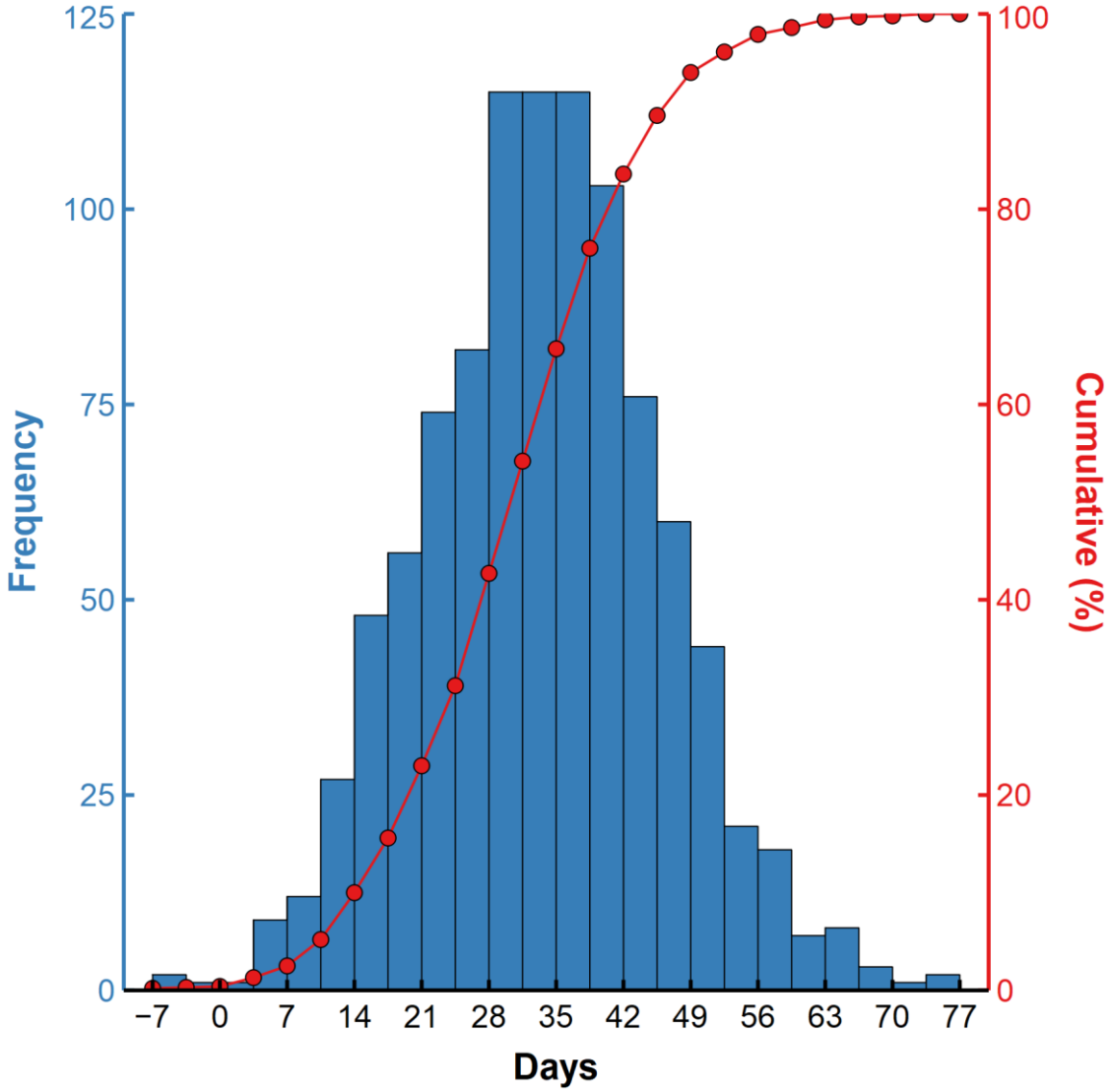

Figure S8. Histogram and cumulative probability of the time interval estimate between Spike 1 and 2 of the large insoluble particle concentrations obtained from 1,000 Monte Carlo simulations.

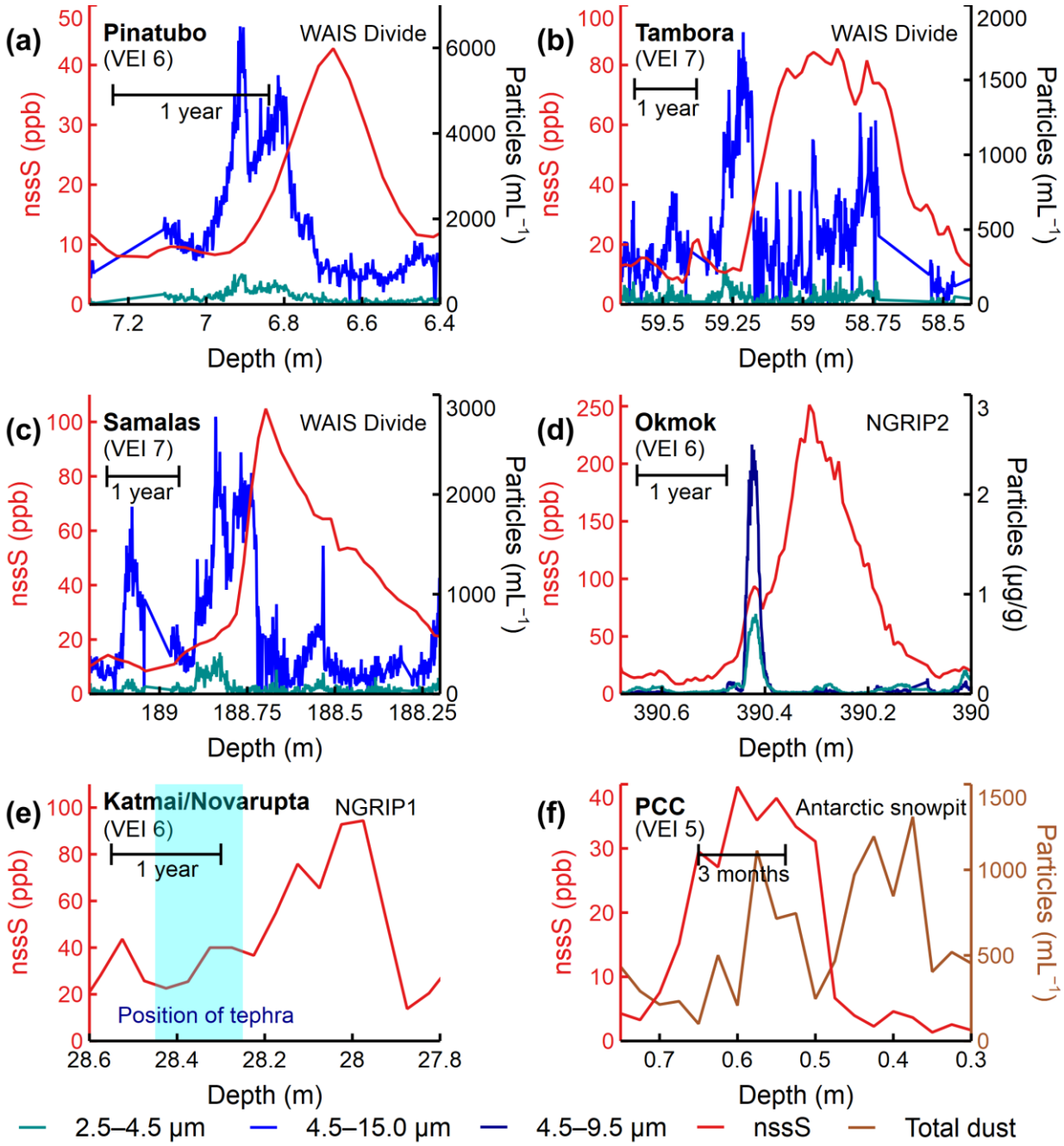

Figure S9. Comparison of depth differences between non-sea-salt sulfur (nssS) and insoluble particles from major volcanic eruptions from previously published records. **(a)–(c)** Particle counts and nssS concentration of 1991 Pinatubo, 1815 Tambora, and 1257 Samalas eruptions from WAIS Divide ice core[30]. **(d)** Particle and nssS concentration of BCE 43 Okmok eruption from NGRIP2 ice core[31]. **(e)** Position of the tephra associated to the 1912 Katmai/Novarupta eruption and nssS concentration from NGRIP1 ice core[32]. **(f)** Total particle counts and nssS concentration of the 2011 Puyehue-Cordón Caulle (PCC) eruption from Antarctic snowpit[33].

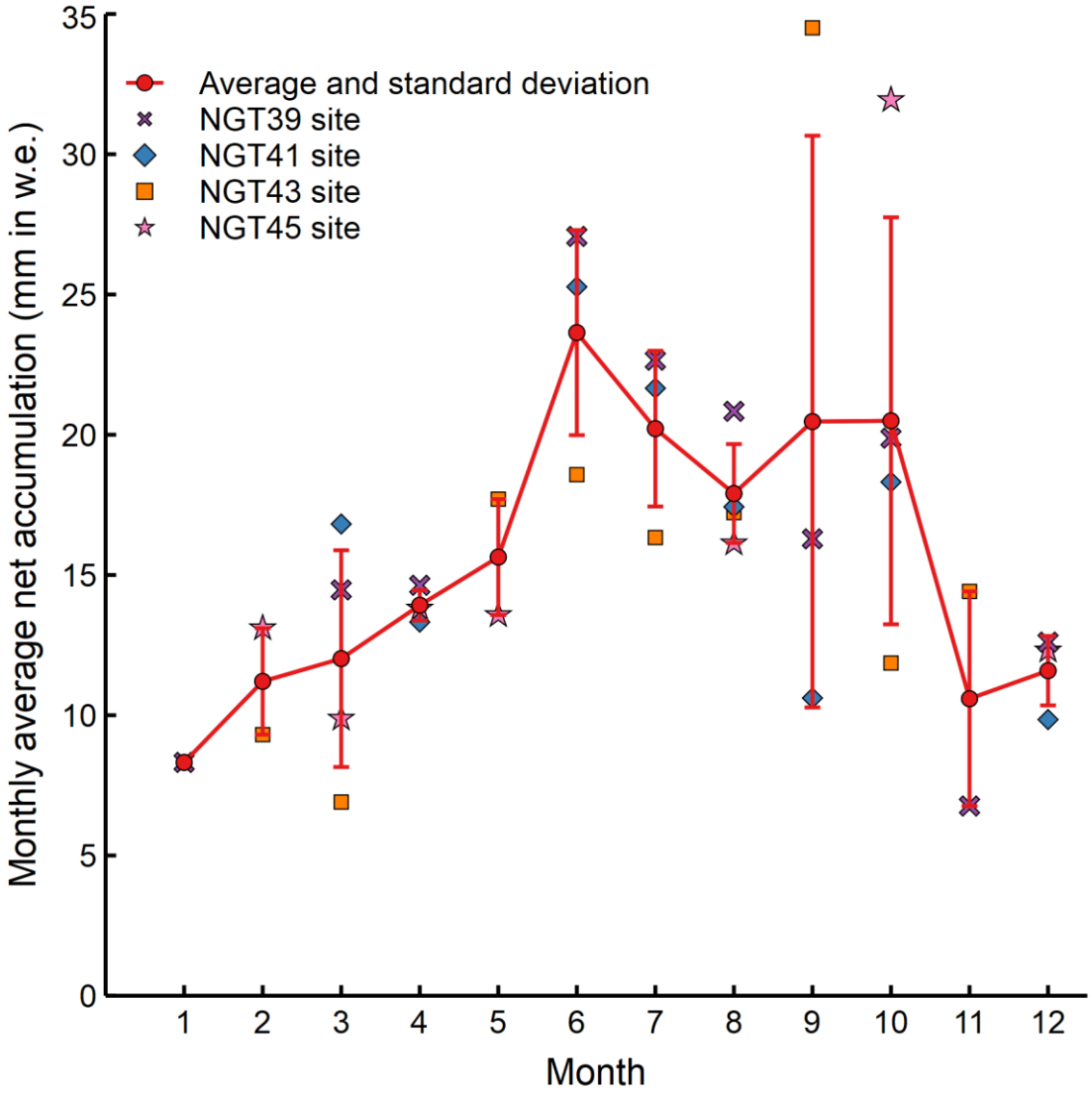

Figure S10. Monthly average net accumulation across the sites (red line) and that of each site (NGT39, NGT41, NGT43, and NGT45) in north central Greenland during 1991–1995[5]. The error bars shown are the standard deviation of all data points for the relevant month (1 σ). See methods section for more information.

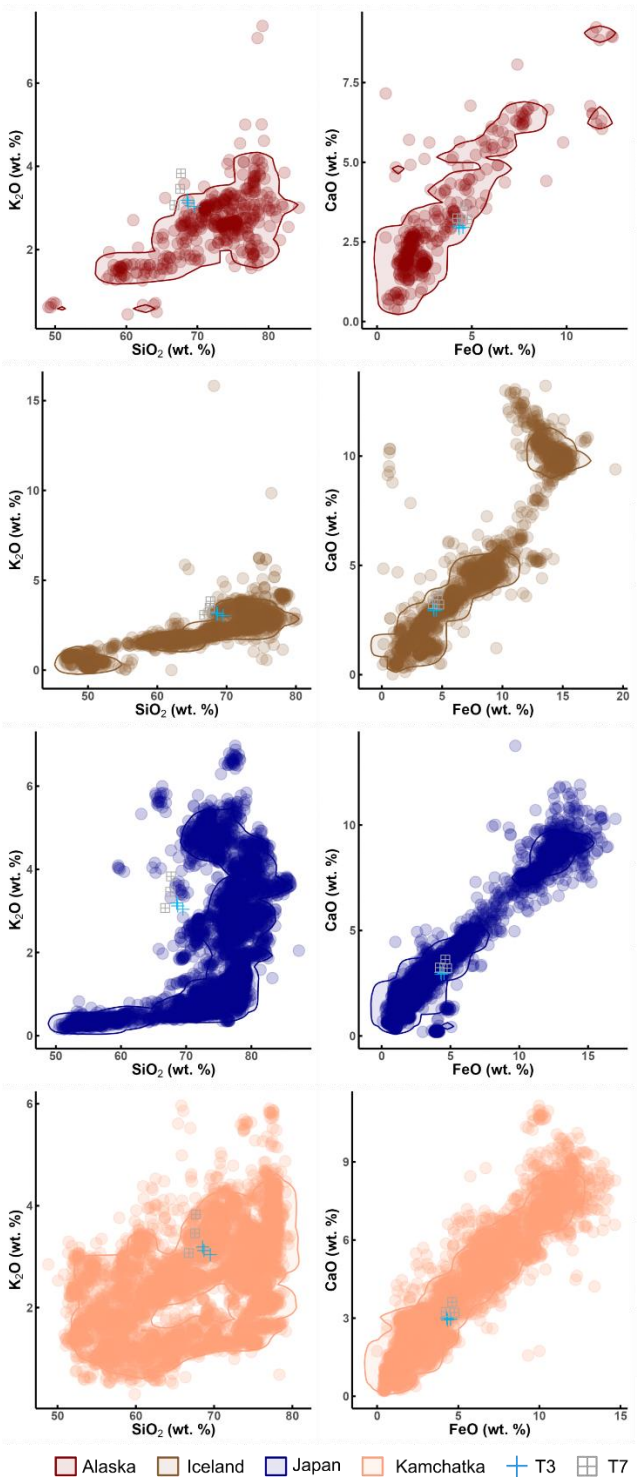

Figure S11. Comparison of chemical composition between tephra population found in sample T3 and T4, and with several regional tephra databases (e.g. Alaska, Iceland, Japan, and Kamchatka). Alaskan data are from Cameron et al.[34]. Icelandic data are from Tephrabase (https://www.tephrabase.org/). Japanese data are from Schindlbeck et al., Chen et al., Albert et al., and Smith et al.[35–38]. Kamchatka data are from Portnyagin et al.[39].

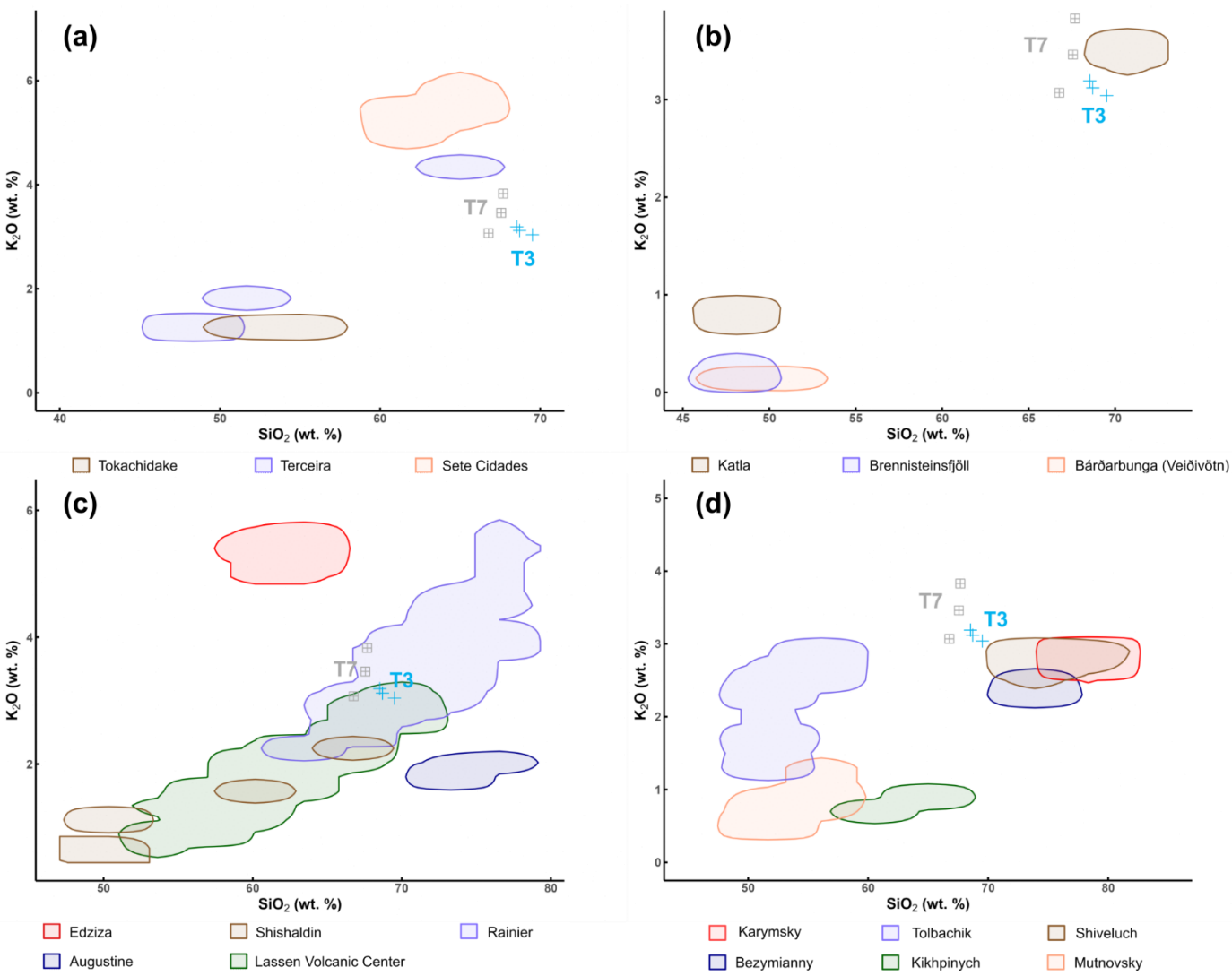

Figure S12. SiO_2 and K_2O bi-plot for tephra populations found in sample T3 and T7, and proximal or distal tephra shards of candidate volcanoes. **(a)** Japan and Portugal, **(b)** Iceland, **(c)** North America, and **(d)** Russia. Refer to Supplementary Table 3 for references. Diagram of candidate volcanoes from Ljósufjöll, Oddnyjarhnjukur-Langjokull, Adatarayama, Kirishimayama, Kuchinoerabujima, Akan, Picos Fissural Volcanic System, Glacier Peak, and Adams were not available because of lack of measurement results.

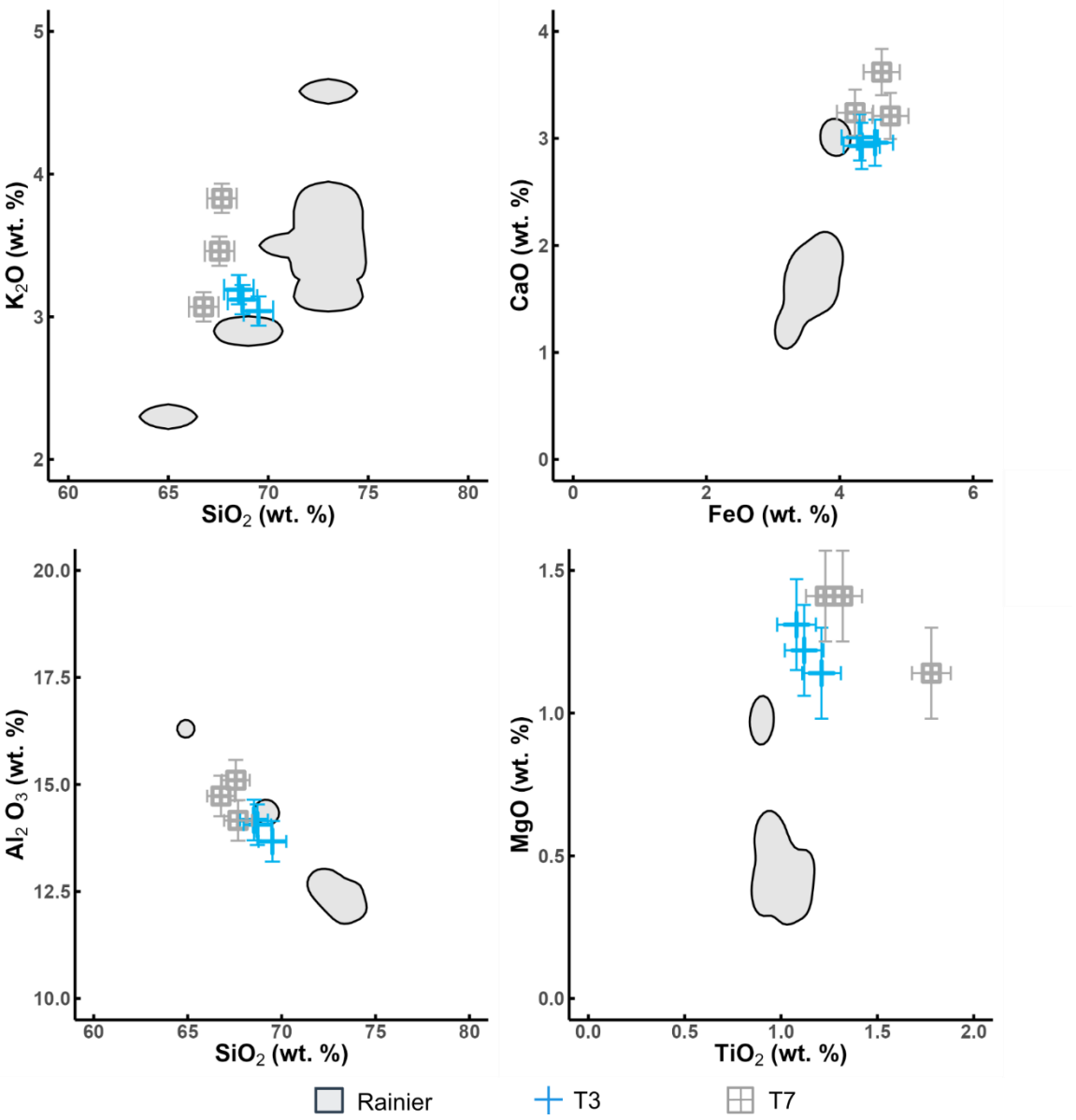

Figure S13. Chemical composition comparison of tephra populations found in sample T3 and T7, and proximal Rainier ash fallouts dated to 1,040 ± 410 cal year BP[1] (i.e. 910 ± 410 CE). The error bars shown indicate 2 σ standard deviation of the St. Helens andesitic ash glass (StHs6/80-G) international secondary glass standard.

Supplementary References

1. Sisson, T. W. & Vallance, J. W. Frequent eruptions of Mount Rainier over the last ~2,600 years. *B. Volcanol.* **71,** 595–618, https://doi.org/10.1007/s00445-008-0245-7 (2009).

2. Plunkett, G. et al. Trace element analysis of Late Holocene tephras from Greenland ice cores. *Quaternary Newsletter* **143,** 10–20 (2017).

3. Sun, C. et al. Ash from Changbaishan Millennium eruption recorded in Greenland ice: Implications for determining the eruption's timing and impact. *Geophys. Res. Lett.* **41,** 694–701, https://doi.org/10.1002/2013GL058642 (2014).

4. Plunkett, G. et al. Smoking guns and volcanic ash: the importance of sparse tephras in Greenland ice cores. *Polar Res.* **39,** https://doi.org/10.33265/polar.v39.3511 (2020).

5. Shuman, C. A., Bromwich, D. H., Kipfstuhl, J., & Schwager, M. Multiyear accumulation and temperature history near the north Greenland ice core project site, north central Greenland. *J. Geophys. Res.-Atmos.* **106,** 33853–33866, https://doi.org/10.1029/2001JD900197 (2001).

6. Kuehn, S. C., Froese, D. G., Shane, P. A. R. & INTAV Intercomparison Participants. The INTAV intercomparison of electron-beam microanalysis of glass by tephrochronology laboratories: Results and recommendations. *Quaternary Int.* **246,** 19–47, https://doi.org/10.1016/j.quaint.2011.08.022 (2011).

7. Holmes, N. et al. Climatic variability during the last millennium in western Iceland from lake sediment records. *The Holocene* **26,** 756–771, https://doi.org/10.1177/0959683615618260 (2016).

8. Óladóttir, B. A., Larsen, G., & Sigmarsson, O. Holocene volcanic activity at Grímsvötn, Bárdarbunga and Kverkfjöll subglacial centres beneath Vatnajökull, Iceland. *Bull. Volcanol.* **73,** 1187–1208, https://doi.org/10.1007/s00445-011-0461-4 (2011).

9. Hudak, M. R., Feineman, M. D., LaFemina, P. C., Geirsson, H. & Agostini, S. Conduit formation and crustal microxenolith entrainment in a basaltic fissure eruption: Observations from Thríhnúkagígur volcano, Iceland. *Volcanica* **5,** 249–270, https://doi.org/10.30909/vol.05.02.249270 (2022).

10. Jennings, A. et al. Holocene tephra from Iceland and Alaska in SE Greenland shelf sediments. *Geological Society, London, Special Publications* **398,** 157–193, https://doi.org/10.1144/SP398.6 (2014).

11. Okumura, K. Quaternary tephra studies in the Hokkaido district, northern Japan. *The Quaternary Research* **30,** 379–390 (In Japanese with English abstract) (1991).

12. Yamagishi, H. & Freebrey, C. Ballistic ejecta from the 1988–1989 andesitic vulcanian eruptions of Tokachidake volcano, Japan: morphological features and genesis. *J. Volcanol. Geoth. Res.* **59,** 269–278, https://doi.org/10.1016/0377-0273(94)90082-5 (1994).

13. Hildenbrand, A., Weis, D., Madureira, P. & Marques, F. O. Recent plate re-organization at the Azores triple junction: Evidence from combined geochemical and geochronological data on Faial, S. Jorge and Terceira volcanic islands. *Lithos* **210,** 27–39, https://doi.org/10.1016/j.lithos.2014.09.009 (2014).

14. Ellis, B. S. et al. Geochemistry of the Pepom tephra deposits: The most recent intracaldera volcanism of Sete Cidades volcano, São Miguel, Azores. *J. Volcanol. Geoth. Res.* **432,** 107673, https://doi.org/10.1016/j.jvolgeores.2022.107673 (2022).

15. Derkachev, A. N. et al. Middle to late Pleistocene record of explosive volcanic eruptions in marine sediments offshore Kamchatka (Meiji Rise, NW Pacific). *J. Quaternary Sci.* **35,** 362–379, https://doi.org/10.1002/jqs.3175 (2019).

16. Shishkina, T. Storage conditions and degassing processes of low-K and high-Al tholeiitic island-arc magmas: Experimental constraints and natural observations for Mutnovsky volcano, Kamchatka. *PhD thesis, Leibniz University of Hannover, Germany* (2012).

17. Kyle, P. R., Ponomareva, V. V. & Schluep, R. R. Geochemical characterization of marker tephra layers from major Holocene eruptions, Kamchatka Peninsula, Russia. *Int. Geol. Rev.* **53,** 1059–1097, https://doi.org/10.1080/00206810903442162 (2010).

18. Ponomareva, V. et al. A full Holocene tephrochronology for the Kamchatsky peninsula region: Applications from Kamchatka to north America. *Quaternary Sci. Rev.* **168,** 101–122, https://doi.org/10.1016/j.quascirev.2017.04.031 (2017).

19. Zelenin, E., Kozhurin, A., Ponomareva, V. & Portnyagin, M. Tephrochronological dating of paleoearthquakes in active volcanic arcs: A case of the eastern volcanic front on the Kamchatka peninsula (northwest Pacific). *J. Quaternary Sci.* **35,** 349–361, https://doi.org/10.1002/jqs.3145 (2019).

20. Smith, H. W., Okazaki, R. & Knowles, C. R. Electron microprobe data for tephra attributed to glacier peak, Washington. *Quaternary Res.* **7,** 197–206, https://doi.org/10.1016/0033-5894(77)90036-9 (1977).

21. Clynne, M. A., Christiansen, R. L., Trimble, D. A., & McGeehin, J. P. Radiocarbon dates from volcanic deposits of the Chaos Crags and Cinder Cone eruptive sequences and other deposits, Lassen Volcanic National Park and vicinity, California. *U.S. Geological Survey Open-file Report 02-290*, 18 p. http://pubs.usgs.gov/of/2002/of02-290/ (2008).

22. Fournelle, J. & Marsh, B. D. Shishaldin Volcano: Aleutian high-alumina basalts and the question of plagioclase accumulation. *Geology* **19,** 234–237, https://doi.org/10.1130/0091-7613(1991)019<0234:SVAHAB>2.3.CO;2 (1991).

23. Bolton, M. S. M. et al. Machine learning classifiers for attributing tephra to source volcanoes: an evaluation of methods for Alaska tephras. *J. Quaternary Sci.* **35,** 81–92, https://doi.org/10.1002/jqs.3170 (2019).

24. Busaccca, A. J., Nelstead, K. T., McDonald, E. V. & Purser, M. D. Correlation of distal tephra layers in loess in the channeled Scabland and Palouse of Washington State. *Quaternary Res.* **37,** 281–303, https://doi.org/10.1016/0033-5894(92)90067-S (1992).

25. Hildreth, W. & Lanphere, M. A. Potassium-argon geochronology of a basalt-andesite-dacite arc system: The Mount Adams volcanic field, cascade range of southern Washington. *Geol. Soc. Am. Bull* **106,** 1413–1429, https://doi.org/10.1130/0016-7606(1994)106<1413:PAGOAB>2.3.CO;2 (1994).

26. Yang, Q. et al. The Millennium eruption of Changbaishan Tianchi volcano is VEI 6, not 7. *B. Volcanol.* **83,** 74, https://doi.org/10.1007/s00445-021-01487-8 (2021).

27. Plummer, C. T. et al. An independently dated 2000-yr volcanic record from Law Dome, East Antarctica, including a new perspective on the dating of the 1450s CE eruption of Kuwae, Vanuatu. *Clim. Past* **8,** 1929–1940, https://doi.org/10.5194/cp-8-1929-2012 (2012).

28. McConnell, J. R. High-resolution elemental and chemical measurements in the NGRIP2 core, North Greenland, 2015. *Arctic Data Center.* https://doi.org/10.18739/A20R9M558 (2023).

29. Sigl, M., & McConnell, J. R. NEEM-2011-S1 ice-core aerosol record (conductivity, NH4, NO3, BC, acidity, Na, Mg, S, Ca, Mn, Sr, Ce) in NW-Greenland at 2 cm resolution from 86-1997 CE on the annual-layer counted NS1-2011 chronology. *PANGAEA*, https://doi.org/10.1594/PANGAEA.940553 (2022).

30. Kreutz, K., & Koffman, B. G. WAIS Divide Microparticle Concentration and Size Distribution, 0-2400 ka. *U.S. Antarctic Program (USAP) Data Center*, https://doi.org/10.7265/N5KK98QZ (2015).

31. McConnell, J. R. et al. Extreme climate after massive eruption of Alaska's Okmok volcano in 43 BC and its effects on the civil wars of the late Roman Republic. *P. Natl. Acad. Sci. USA.* **117,** 15443–15449, https://doi.org/10.1073/pnas.2002722117 (2020).

32. Coulter, S. E. et al. Holocene tephras highlight complexity of volcanic signals in Greenland ice cores. *J. Geophys. Res.-Atmos.* **117,** https://doi.org/10.1029/2012JD017698 (2012).

33. Koffman, B. G., & Kreutz, K. Snowpit evidence of the 2011 Puyehue-Cordon Caulle (Chile) eruption in West Antarctica. *U.S. Antarctic Program (USAP) Data Center*, https://doi.org/10.15784/601036 (2017).

34. Camon, C. E., Crass, S. W., & AVO staff. Geologic Database of Information on Volcanoes in Alaska (GeoDIVA): Digital Data Series DDS 20, Alaska Division of Geological & Geophysical Surveys, Fairbanks, Alaska, United States, https://doi.org/10.14509/30901 (2022).

35. Schindlbeck, J. C. et al. One Million Years tephra record at IODP Sites U1436 and U1437: Insights into explosive volcanism from the Japan and Izu arcs. *Isl. Arc* **27,** e12244, https://doi.org/10.1111/iar.12244 (2018).

36. Chen X.-Y. et al. Developing a Holocene tephrostratigraphy for northern Japan using the sedimentary record from Lake Kushu, Rebun Island. *Quaternary Sci. Rev.* **215,** 272–292, https://doi.org/10.1016/j.quascirev.2019.05.017 (2019).

37. Albert, P. G. et al. Geochemical characterisation of the Late Quaternary widespread Japanese tephrostratigraphic markers and correlations to the Lake Suigetsu sedimentary archive (SG06 core). *Quat. Geochronol.* **52,** 103–131, https://doi.org/10.1016/j.quageo.2019.01.005 (2019).

38. Smith, V. C. et al. Identification and correlation of visible tephras in the Lake Suigetsu SG06 sedimentary archive, Japan: chronostratigraphic markers for synchronising of east Asian/west Pacific palaeoclimatic records across the last 150 ka. *Quaternary Sci. Rev.* **67,** 121–137, https://doi.org/10.1016/j.quascirev.2013.01.026 (2013).

39. Portnyagin, M. V. et al. TephraKam: geochemical database of glass compositions in tephra and welded tuffs from the Kamchatka volcanic arc (northwestern Pacific). *Earth Syst. Sci. Data* **12,** 469–486, https://doi.org/10.5194/essd-12-469-2020 (2020).